Ion impact cross-sections for ADAS applications

The bigger picture

Hugh Summers and the ADAS team

University of Strathclyde/CCFE Culham/JET

ADAS workshop
30 Sep 2014
Warsaw

Ion impact Vs electron impact

Some 90% of the ADAS reaction database (~10Gbyte) is composed of electron impact excitation collision cross-sections or Maxwell collisional rate coefficients. Of the remaining 10%, almost all is composed of state-selective charge transfer cross-sections. Why is this so?

The vast preponderance of binary encounter collisions between ions and electrons in a plasma are elastic - exchanging kinetic energy between the reactants, but not exciting the reactants – and so are have been of no interest to ADAS, although central to plasma kinetic theory and transport.

Ion impact excitation cross-sections with ion targets look a bit different from electron impact cross-sections with ion targets

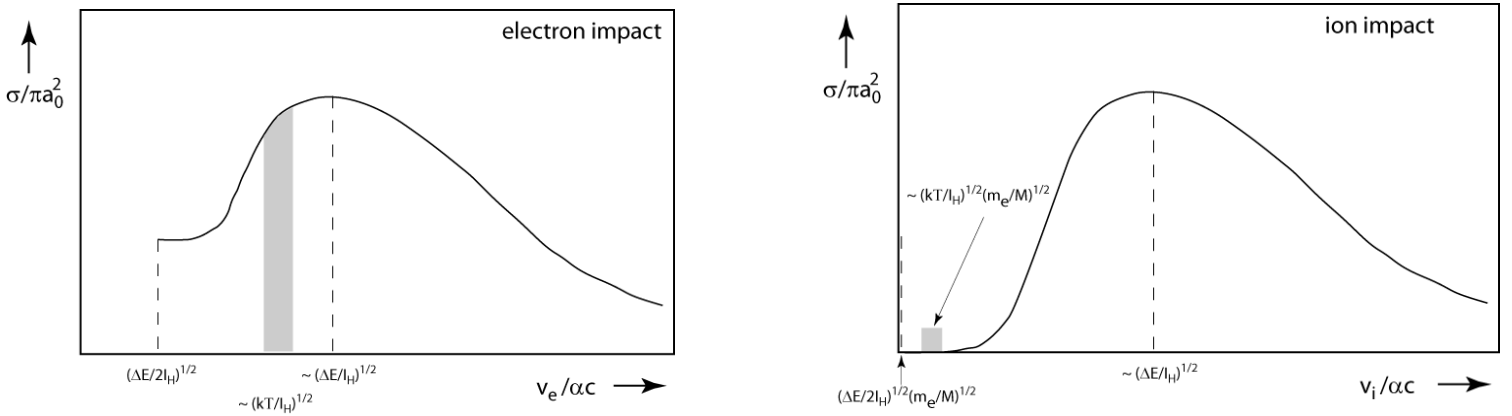

In a thermal plasma with the electrons and ions at the same Maxwellian temperature, the typical electron and ion projectile speeds are positioned on the cross-section Vs speed curves as shown.

Situations favouring ion impact collisions (a)

Excitation reactions of very small energy transfer relative to the ionisation potential of the target.

- fine structure transitions within a term

With ITER our interest is moving to heavier elements and higher ion charge states so the fine structure energy separations become significant in CR modelling.

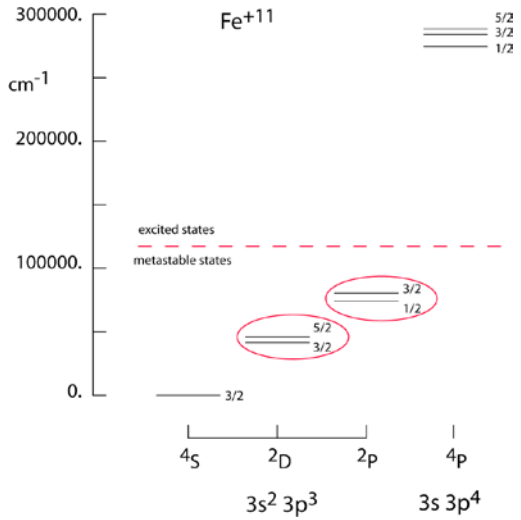

Quadrupole transitions: isolated-atom target states

- Rydberg l-redistributive transitions

For the higher charge state ions, the Rydberg states matter for recombination, but for coupling to low-level fine structure an nl-resolved picture is best

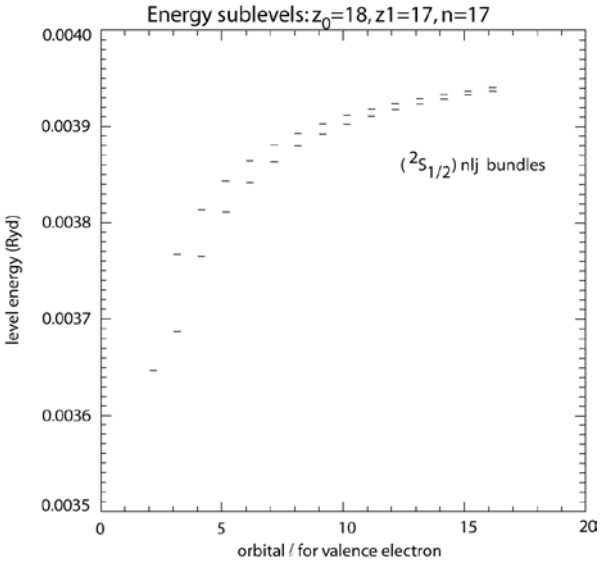

Dipole transitions: isolated-atom target states

Situations favouring ion impact collisions (b)

Fast ion projectiles with speeds greater than ~50 times the thermal average speed or equivalently fast target ions/atoms.

- accelerated ions, fast alphas, ionised beam atoms

With fast ion spectroscopy and especially FICXS, it is appropriate to give more attention to the reactive interactions of such fast ions.

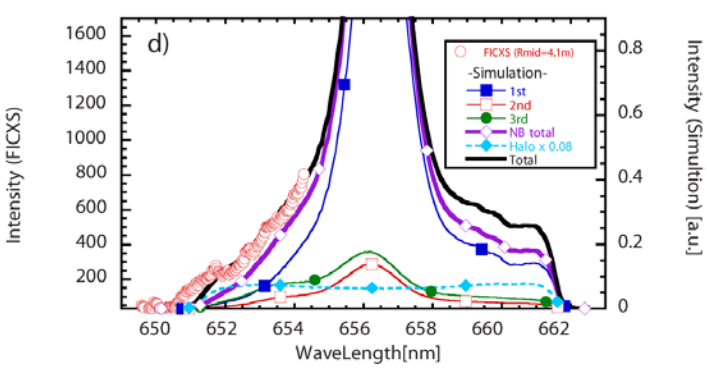

Various

- neutral beams

The ITER heating beams at ~1MeV move away from the linear threshold variation of energies with electric field strength.

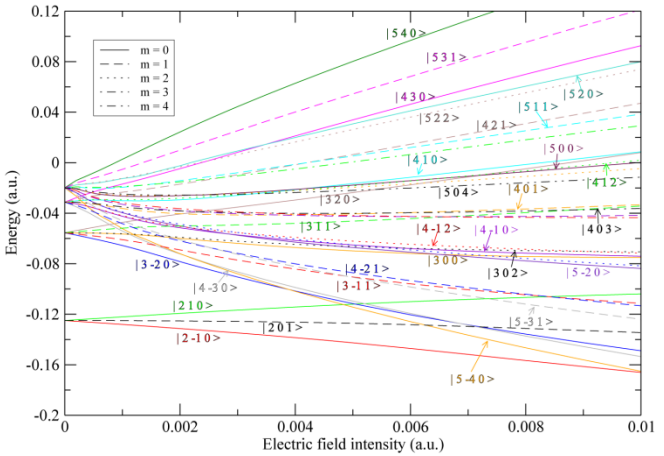

Dipole transitions: Stark manifold target states

Fig. 1 – see Osakabe et al. (2008) Rev. Sci. Instr. 79 (10). Fig 2. – see Menchero & Summers Phys. Rev. A, 88 (2013) 022509.

On Coulomb collisions and cross-sections

- For electron collisions with ions, ADAS has focussed on a quantum mechanical description of the collisions, evaluated preferably in a close- coupling partial wave analysis.

- For ion impact, because of the mass factor, an impractically large number of partial waves would need to be included in the close coupling region near the target .

- In these circumstances, the classical projectile picture with the projectile following a classical trajectory in a Coulomb field is helpful.

- The Classical Coulomb scattering picture for elastic scattering is central to the estimation of elastic scattering angles, mean energy transfers etc. Between plasma ions and electrons. It has also a long history for inelastic collisions.

- Our intention is to use the classical trajectory impact parameter approach for the types of excitation collision summarised earlier.

- We shall use it for both electrons and ions and do will so in a relativistically correct manner, since for ITER electron temperatures above 25keV, this is now required.

- We shall exploit the impact parameter picture to provide angular differential cross-sections for modelling, and scale the impact parameter cross-sections with best available total cross-sections.

Scattering angles, energy transfer and reaction rates

Specifying the orbit parameter $a = \left| z_p z_t \right| / E_p$ then $\tan(\theta/2) = a/p$

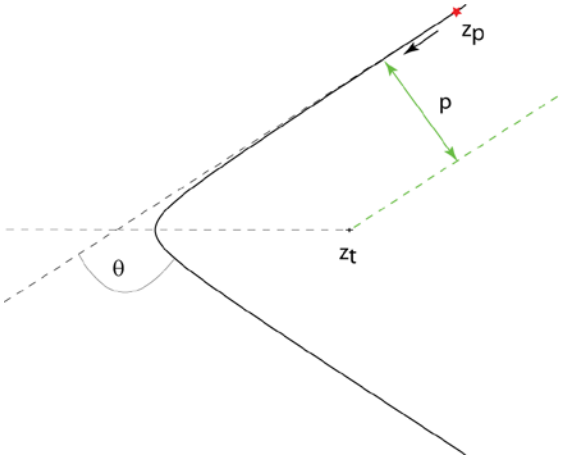

What we need from this is the connection between the scattering angle in the laboratory frame (*lab*)and that in the centre of mass frame (*cms*) and the kinetic energy change of the projectile in the *lab* frame which are familiar from basic binary collision dynamics.

The relativistically correct expressions require a little more care with the Lorentz transformation between the *lab* and *cms* frames.

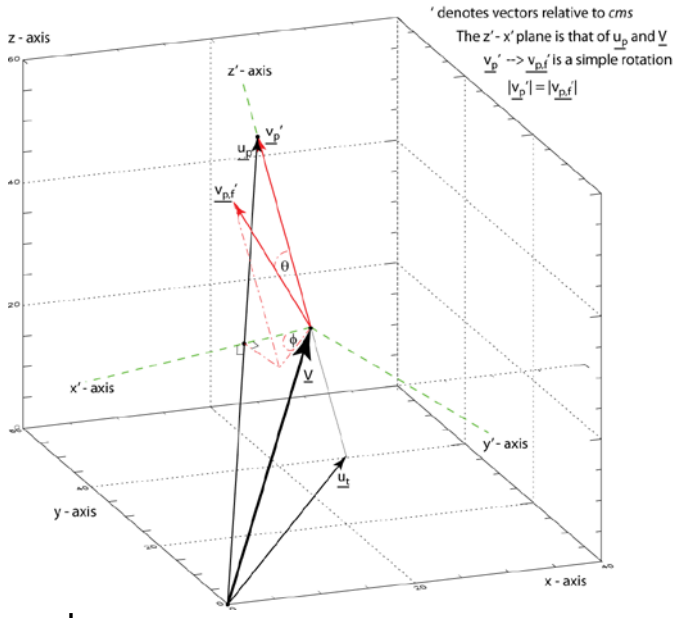

The relativistic reaction rate is

$$R_{t,p} = \left[N_t N_p\right]_{lab} \iint \frac{\left[c\beta_R \sigma(v_R)\right]_{cms} \gamma_R}{\beta_t \beta_p} f_t(\underline{p_t}) f_p(\underline{p_p}) \underline{dp_t}\, \underline{dp_p}$$

where the f's are the distributions in the lab frame – most often isotropic relativistic Maxwellians. In the latter case

$$R_{t,p} = \left[N_t N_p\right]_{lab} \frac{\phi_t \phi_p c}{K_2(\phi_t) K_2(\phi_p)} \int \frac{\sigma(\gamma_R)\beta_R^2 \gamma_R^2 K_1(z)}{z} d\gamma_R$$

with $z = \sqrt{\phi_t^2 + 2\phi_t\phi_p\gamma_R + \phi_p^2}$, also the relativistic reduced mass is used.

Lengths are in Bohr radii and energies in Rydbergs. Relativistic speeds are in terms of β=v/c with $\gamma = 1/\sqrt{1-\beta^2}$. Also use $\phi = mc^2/kT$

Some history of Coulomb excitation

- On the basis of the last slide, our problem has been reduced to solving the one-body classical trajectory problem for the cross-sections (differential and total) for arbitrary mass positive and negative charge colliders in the *cms* frame using the correct reduced mass collider with the centre of mass at rest. Relativistic mass variation in the orbit may be neglected.

- The definite work on Coulomb excitation is Alder et al. (1956) Rev. Mod. Phys. 28,432.

- It was applied to excitation by electrons of quadrupole transitions in neutral atoms by Seaton (1962) Mon. Not. R. Astr. Soc. 79, 1105.

- Burgess (see Burgess& Percival (1968) Adv. At. & Mol. Phys. 4, 109) extended the application to dipole excitation of ions by electrons.

- Burgess & Summers (1976)Mon. Not. R. Astr. Soc. 174,345 unified the approach for ion and electron impact (c.f. ADAS ipprog).

- Bely and Faucher programmed the quadrupole, proton impact case from Alder et al. tables. There have been several variations and extensions over the years, including Bahcall & Wolf, Faucher, Reid & Ryans.

- A re-examination was carried out by Burgess & Tully (2005) J. Phys. B. 38,2644 of the proton impact quadrupole case with special attention to the high energy behaviour. Several errors were found in the previous work.

- The ADAS objective is to rebuild the complete picture – dipole and quadrupole, positive and negative colliders, relativistically correct, high energy behaviour correct – stepping forward from Burgess & Tully.

Calculation aspects (a)

Working now in the centre of mass frame, the Rutherford elastic differential cross-section is

$$\frac{d\sigma}{d\Omega} = \frac{1}{4\pi}\left(\frac{z_t z_p}{E_p}\right)^2 \mathrm{cosec}^4(\theta/2)$$

The differential excitation and total excitation cross-sections for an $i \to j$ electronic transition in the target ion

$$\frac{d\sigma_{i\to j}}{d\Omega} = \frac{1}{4\pi}\left(\frac{z_t z_p}{E_p}\right)^2 P_{i\to j}(\theta)\mathrm{cosec}^4(\theta/2) \quad \text{and} \quad \sigma_{i\to j} = \frac{1}{2}\left(\frac{z_t z_p}{E_p}\right)^2 \int_0^\pi P_{i\to j}(\theta)\mathrm{cosec}^4(\theta/2)\sin\theta d\theta$$

In turn the probabilities are

$$P_{i\to j} = \frac{1}{\omega_i}\sum_{M_i M_j}\left|b_{ij}(t=\infty)\right|^2 \quad \text{with} \quad i\dot{b}_{ij}(t) = \frac{1}{2}\sum_k \left\langle j\left|H'\right|k\right\rangle e^{i(E_j-E_k)t/2} b_{ik}(t) \quad \text{and} \quad b_{ik}(t=-\infty) = \delta_{ik}$$

In perturbation theory

$$b_{ij}(t=\infty) = \frac{1}{2i}\int_{-\infty}^{\infty}\left\langle j\left|H'\right|i\right\rangle e^{i(E_j-E_i)t/2} dt$$

Calculation aspects (b)

We are concerned with dipole and quadrupole transitions in the electronic structure of the complex target ion.

The interaction Hamiltonian is $H' = 2z_p \sum_{i=1}^{N} \left\{ \frac{1}{|\underline{r}_i - \underline{r}_p|} - \frac{1}{r_p} \right\}$ for which we require the multipole expansion

$$\frac{1}{|\underline{r} - \underline{r}_p|} = \sum_{\lambda=0}^{\infty} \frac{4\pi}{2\lambda+1} \sum_{\mu=-\lambda}^{\lambda} Y^*_{\lambda\mu}(\hat{\underline{r}}) Y_{\lambda\mu}(\hat{\underline{r}}_p) \frac{r_<^\lambda}{r_>^{\lambda+1}}.$$ For non-penetrating orbitals $\frac{r_<^\lambda}{r_>^{\lambda+1}} = \frac{r^\lambda}{r_p^{\lambda+1}}$

The transition probability in perturbation theory may be written as

$$P_{J_i \to J_j}(\theta) = 16\pi z_p^2 \sum_{\lambda=1}^{\infty} \left(\frac{1}{2\lambda+1} \right)^3 B(E\lambda) \sum_{\mu} \left| S_{E\lambda\mu} \right|^2$$

The atomic part is $B(E\lambda) = \frac{1}{2J_i+1} \left| \left\langle J_i \| M(\lambda) \| J_j \right\rangle \right|^2$ in terms of the reduced multipole operator

which in our dipole and quadrupole cases are expressible in terms of the associated transition probabilities.

Calculation aspects (c)

The projectile multipole path integral part as a function of time is usually expressed in the hyperbolic path coordinate ω appropriately for the repulsive and attractive cases

$$S_{E\lambda\mu} = \frac{(-1)^{(\lambda+\mu)/2} m^{1/2}}{\sqrt{E_p}\, a^{\lambda}} \left(\frac{2\lambda+1}{4\pi}\right)^{1/2} \frac{[(\lambda-\mu)!(\lambda+\mu)!]^{1/2}}{(\lambda-\mu)!!(\lambda+\mu)!!} I_{\lambda\mu}(\theta,\xi) \qquad \lambda+\mu \text{ even}$$

$$= 0 \qquad \lambda+\mu \text{ odd}$$

$\xi = \left|z_p z_t\right| m^{1/2} \dfrac{\Delta E_{ij}}{2\sqrt{E_p}}$ is the adiabaticity parameter.

One of the most computationally useful forms of the $I_{\lambda\mu}(\theta,\xi)$ is

$$I_{\lambda\mu}(\theta,\xi) = e^{\mp\pi\xi/2} \int_{-\infty}^{\infty} e^{-\xi\varepsilon\cosh\omega \pm i\xi\omega} \frac{\left[i\sinh\omega \pm \varepsilon - (\varepsilon^2-1)^{1/2}\cosh\omega\right]^{\mu}}{\left[i\varepsilon\sinh\omega \pm 1\right]^{\lambda+\mu}} d\omega$$

where the $\pm$ denotes the repulsive(+) and attractive(-) cases. Note $I_{\lambda\mu}^{attractive}(\theta,\xi) = (-1)^{\lambda} e^{\pi\xi} I_{\lambda-\mu}^{repulsive}(\theta,\xi)$

and the dipole analytic form $I_{1\pm1}^{repulsive}(\theta,\xi) = -2\xi e^{-(\pi/2)\xi}\left[K'_{i\xi}(\xi\varepsilon) \pm \dfrac{(\varepsilon^2-1)^{1/2}}{\varepsilon} K_{i\xi}(\xi\varepsilon)\right]$

Comments

- The figure shows an illustration of the $I_{\lambda\mu}$ integrals which are obtained to high precision.

- With the probabilities $P_{i\to j}$ as a function of scattering angle θ or impact parameter p, we can obtain the total cross-section and assess some of the issues which distinguish the perturbative solutions.

- The schematic of hyperbolic trajectories of varying impact parameter is helpful. 1 is a distant encounter with P small, 2 marks the start of the strong coupling region with P~1/2 (if it occurs) and the breakdown of perturbation theory. The boundary of the atom is indicated by 3, while 4 is a penetrating trajectory. At high collision energy, P remains small and decreases with energy for all trajectories. Special treatment is imposed for closest approaches < r_s and/or r_w.

- The failure of some of the older methods is because of their treatment inside r_w. As long as P, at finite r_w, is incorporated, the high energy behaviour is correct, but not the exact numerical form.

- Since the quantum mechanical Born approximation is valid and the same for ions and electron projectiles of the same speed, r_w can be chosen so that the Born behaviour is numerically matched at high energy. The Born limits are available from our structure codes.

- Attempts to handle penetrating orbits with $r_<$ and $r_>$ are unconvincing in the simple Coulomb excitation approach.

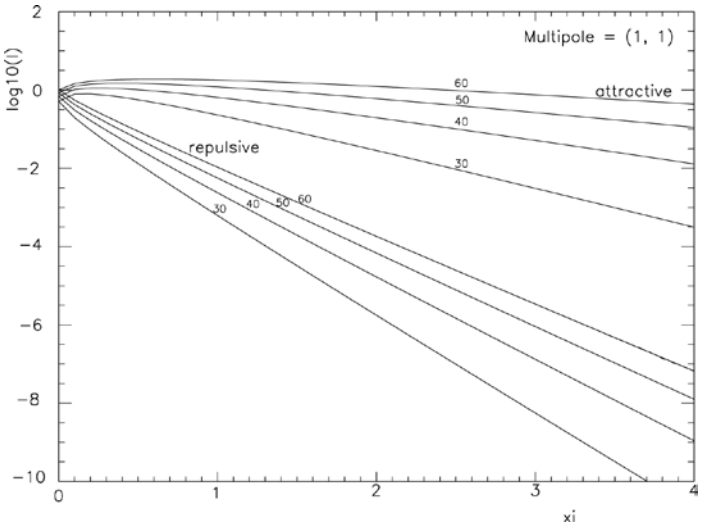

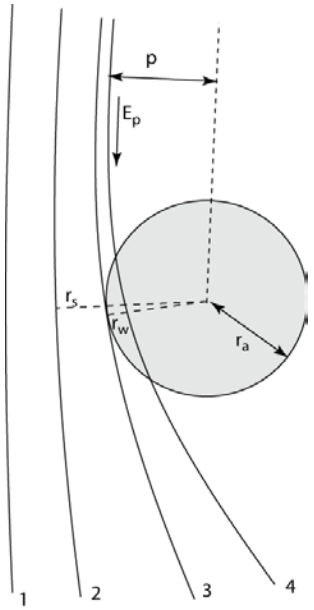

The road map (a)

- GCR processing for including ion impact quadrupole transitions
- Handles electron and ion impact
- Valid in the kinematic relativistic regime
- Convenient inclusion of ion impact on the fly at the GCR processing stage – no archiving.
- Note new outputs for Monte Carlo modelling which includes differential cross-sections.
- Impact parameter Coulomb excitation theory carries the relativistic and differential behaviour.

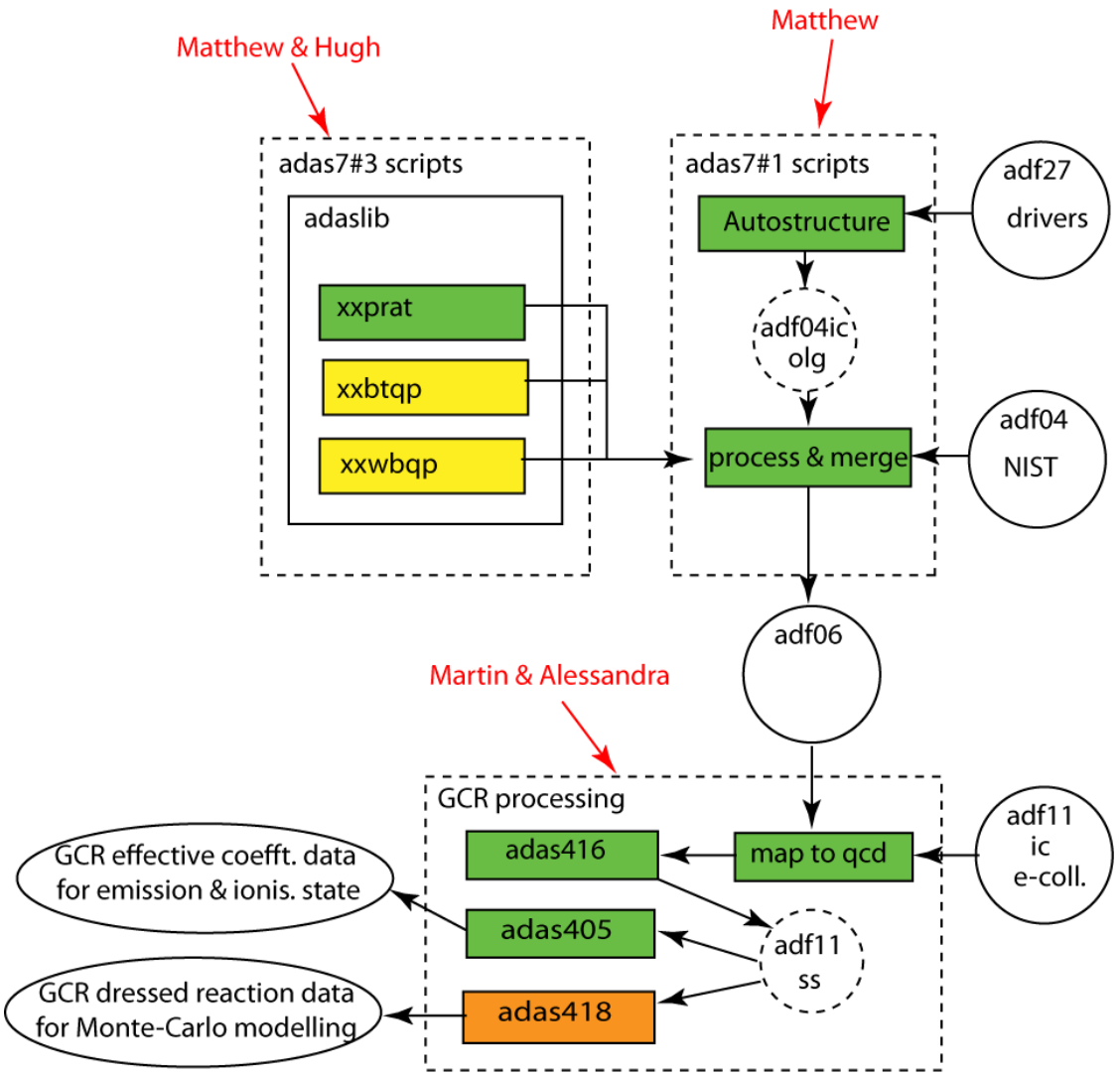

The road map (b)

Right side

- GCR processing for including ion impact dipole transitions between high Rydberg *nlj* substructure
- Handles electron and ion impact
- Valid in the kinematic relativistic regime
- Rydberg explicit lj-mixing creates improved precision projection matrices for ic resolution GCR modelling.

Left side

- Zeroth order Stark manifold basis valid at arbitrary motional-Stark field strengths.
- Beam modelling includes cone of attack effects in ion impact and field ionisation.